Science of the Total Environment 663 (2019) 453–464

Contents lists available at ScienceDirect

Science of the Total Environment

journal homepage: www.elsevier.com/locate/scitotenv

Heterogeneous activation of peroxymonosulfate using Mn-Fe layered double hydroxide: Performance and mechanism for organic pollutant degradation

Lihua Hou [a,b], Xiaoming Li [a,b,*], Qi Yang [a,b,*], Fei Chen [c], Shana Wang [a,b], Yinghao Ma [a,b], You Wu [a,b], Xiaofei Zhu [a,b], Xiaoding Huang [a,b], Dongbo Wang [a,b]

[a] College of Environmental Science and Engineering, Hunan University, Changsha 410082, PR China
[b] Key Laboratory of Environmental Biology and Pollution Control (Hunan University), Ministry of Education, Changsha 410082, PR China
[c] CAS Key Laboratory of Urban Pollutant Conversion, Department of Chemistry, University of Science & Technology of China, Hefei 230026, China

HIGHLIGHTS

- MnFe-LDH was used as heterogeneous catalyst to active peroxymonosulfate.
- The MnFe-LDH/PMS system showed high performance for organic pollutant degradation.
- Rreaction parameters of MnFe-LDH/PMS system for AO7 degradation were optimized.
- Catalyst showed stable catalytic performance in consecutive runs.
- The probable degradation pathways were proposed and discussed.

GRAPHICAL ABSTRACT

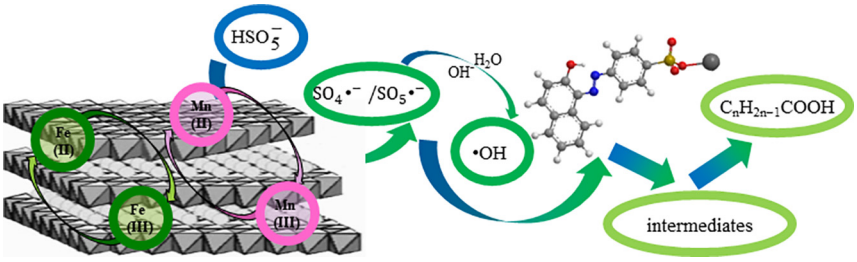

ARTICLE INFO

Article history:
Received 2 November 2018
Received in revised form 14 January 2019
Accepted 15 January 2019
Available online 16 January 2019

Editor: Zhen (Jason) He

Keywords:
Sulfate radical
Heterogeneous activation
Peroxymonosulfate
Reaction mechanism
Degradation pathway

ABSTRACT

On account of high oxidation ability of sulfate radical-based advanced oxidation processes (AOPs), the eco-friendly catalysts for peroxymonosulfate (PMS) activation have received considerable attentions. Previous studies mainly focused on Cobalt-based catalyst due to its high activation efficiency, such as Co_3O_4/MnO_2 and FeCo-layered double hydroxide (LDH), whereas Cobalt-based catalyst usually has serious risk to environment. To avoid this risk, MnFe-LDH was primarily synthesized in this research by simple co-precipitation and subsequently utilized as an effective catalyst for peroxymonosulfate (PMS) activation to degrade organic pollutants. The experimental results demonstrated that MnFe-LDH with a lower dosage (0.20 g/L) could efficiently activate PMS to achieve 97.56% removal of target organic pollutants Acid Orange 7 (AO7). The AO7 degradation process followed the pseudo-first-order kinetic well with an activation energy of 21.32 kJ/mol. The intrinsic influencing mechanism was also investigated. The quenching experiment and electron spin resonance (ESR) indicated that sulfate and hydroxyl radicals were produced by the effective activation of PMS by MnFe-LDH, resulting in a high rate of decolorization. The possible AO7 removal pathway in the constructed MnFe-LDH/PMS system was presented on the basis of UV–vis spectrum analysis and GC–MS, which suggested that the AO7 degradation was firstly initiated by breaking azo linkages, then generated phenyl and naphthalene intermediates and finally presented as ring-opening products. This effective MnFe-LDH/PMS system showed great application potential in the purification of wastewater contaminated by refractory organic pollutants.

© 2019 Elsevier B.V. All rights reserved.

* Corresponding authors at: College of Environmental Science and Engineering, Hunan University, Changsha, Hunan 410082, China.
E-mail addresses: xmli@hnu.edu.cn (X. Li), yangqi@hnu.edu.cn (Q. Yang).

https://doi.org/10.1016/j.scitotenv.2019.01.190
0048-9697/© 2019 Elsevier B.V. All rights reserved.

1. Introduction

Advanced oxidation processes (AOPs), as a competitive alternative to industrial wastewater treatment, have attracted immense interests in recent decades, because of their high degradation efficiency for refractory organic pollutants (Liu et al., 2016; Boczkaj and Fernandes, 2017). In the process, oxidizing free radicals with the high standard oxidation-reduction potential are the main reason for the degradation of organic contaminants, such as sulfate radical (SO_4•$^-$, 2.5–3.1 V) and hydroxyl radical (•OH, 1.9–2.7 V) (Yang et al., 2015b). Peroxymonosulfate (PMS), for its environmental friendliness, security, stability and easy activation (Oh et al., 2016; Zhao et al., 2018), is frequently used to produce sulfate radicals and hydroxyl radicals through the activation of transition metals (Gong et al., 2017; Rastogi et al., 2009), base (Furman, 2010), chemicals (Zhou et al., 2015), heat (Ji et al., 2015), UV (Fang and Shang, 2012) and ultrasound (Cai et al., 2015). Among those activation agents, transition metal was widely used for its simple operation and low running cost as well as high efficiency (Oh et al., 2016; Xiong et al., 2014). Generally, the transition metal activation process was carried out in a heterogeneous system in favor of recovering the solid catalyst, which might cause secondary pollution. In the spectrum of transition metal, cobalt (Co) has been perceived as the most effective one for PMS activation (Gerken et al., 2011; Guo et al., 2013). Liang et al. found that Co_3O_4/MnO_2 had a much high catalytic performance for PMS activation to degrade phenol (Liang et al., 2012). However, Co leaching from catalyst during the process of PMS activation poses a strong threat to human health and the ecological environment, because Co^{2+} is high poisonous and potential carcinogenic even in a very low concentration (Bennekou, 2012; Feng et al., 2017). To avoid this risk, the non-toxic, cheapness, and environmental friendliness mixed metal catalysts of iron and manganese have been extensively investigated to activate PMS (Ghanbari and Moradi, 2017). Yao et al. found that the degradation efficiency of aqueous organic pollutants was low by $MnFe_2O_4$ activated PMS, and the degradation performance could be greatly improved when $MnFe_2O_4$ was immobilized on reduced graphene oxide (Yao et al., 2014). Liu et al. reported that Fe_3O_4-MnO_2 nanocomposites expressed good catalytic activity for the degradation of 4-chlorophenol by PMS only in neutral condition (Liu et al., 2015). Fu et al. synthesized graphitized hierarchical porous biochar (MS) and $MnFe_2O_4$ magnetic composites ($MnFe_2O_4$/MS) to activate PMS for the orange II removal, indicating that $MnFe_2O_4$/MS had high catalytic activity but poor reusability (Fu et al., 2019).

Layered double hydroxides (LDHs), the alkaline inorganic layered compounds with special structures, have received high attention recently and widely applied in catalysis, electrocatalysis, photocatalysis and so on (Bukhtiyarova, 2019). The general chemical formula of LDHs can be written as $[M(II)_{1-x}M(III)_x(OH)_2]^{x+}[A_{x/n}^{n-}]^{x-}\cdot mH_2O$, where M (II) and M(III) are the divalent and trivalent cations, and A^{n-} represents an interlayer anion (Zhao et al., 2018). LDHs have been studied as heterogeneous catalysts to activate PMS because of its simple synthesis method, large surface area and stable structure. Zhao et al. reported that CoMn-LDH exhibited high stability, wide application range of pH and better decomposition efficiency for the remediation of organic dyes (Zhao et al., 2018). Gong et al. synthesized FeCo-LDH and found it had a superior activation property for PMS to degrade RhB because the Fe and Co species could reversibly oxidized and reduced due to the unique structure of LDHs (Gong et al., 2017).

Based on the understanding of good catalytic activity of the mixed metal catalysts of iron and manganese in Fenton-like system and the LDHs's advantages, MnFe-LDH might be a promising catalyst for PMS activation, which could be applied for the degradation of organic pollutants. Up to now, little information was available for MnFe-LDH used for the activation of PMS, which characterized with simple synthesis, high degradation efficiency, wide pH applicability and excellent reusability. In this works, MnFe-LDH was synthesized by a simple co-precipitation method and then utilized as an effective catalyst for peroxymonosulfate (PMS) activation to degrade organic pollutants. The common azo industrial dye, acid organic 7 (AO7, $C_{16}H_{11}N_2NaO_4S\cdot 5H_2O$) was chosen as a targeted recalcitrant organic contaminant to evaluate the catalytic properties of MnFe-LDH. The objectives were to 1) explore an efficient and stable heterogeneous catalyst to increase the activation efficiency of PMS; 2) discuss the influences of several main factors on AO7 degradation, including PMS concentration, catalyst dosage, reaction temperature, solution initial pH, initial AO7 concentration and co-anions; 3) investigate the stability and reusability of MnFe-LDH; 4) explore the mechanism and degradation pathway of AO7 in MnFe-LDH/PMS system. This work could provide a safe, viable and economic technology for the treatment of organic wastewater.

2. Experimental

2.1. Materials

All materials were employed as analytical grade and deionized water was used in all solutions. Manganese (II) nitrate hydrate ($Mn(NO_3)_2\cdot xH_2O$), iron(III) nitrate nonahydrate ($Fe(NO_3)_3\cdot 9H_2O$), sodium hydroxide (NaOH), sodium carbonate (Na_2CO_3), methanol (CH_3OH), tert-butyl alcohol (TBA) ($(CH_3)_3OH$) and phenol (C_6H_5OH) were purchased from Sinopharm Chemical Reagent Co., Ltd. AO7 ($C_{16}H_{11}N_2NaO_4S\cdot 5H_2O$) was purchased from Shanghai chemistry Company No. 3 (Shanghai, China). PMS ($2KHSO_5\cdot KHSO_4\cdot K_2SO_4$, 95% purity), in which the effective constituent is the $KHSO_5$ (≥47% pure), was obtained from DuPont.

2.2. Catalyst preparation

The MnFe-LDH was synthesized using a coprecipitation method. Initially, $Fe(NO_3)_3\cdot 9H_2O$ (1 mmol) and $Mn(NO_3)_2\cdot xH_2O$ (0.25–8.00 mmol) were dispersed into 100 mL of de-ionized water and stirred at a constant speed for 30 min to form solution A. Simultaneously, solution B was formed by dissolving NaOH (0.035 mol) and Na_2CO_3 (0.015 mol) in 100 mL of deionized water. Then, solution B was dripped slowly into solution A and the pH value of resulting suspension was strictly adjusted to 10.4–10.7. The mixture was ultrasonic processed at room temperature for 30 min and then stirred in water bath at 65 °C for 4 h. Lastly, the products MnFe-LDH were acquired by centrifuging (5000 r/min for 5 min), washing and drying in a vacuum oven at 60 °C for 24 h.

2.3. Characterizations

Catalysts were collected in powder form and analyzed by the following methods. X-rays diffractometer (XRD) was recorded on a Japsn Map AHF X-ray diffract to meter (Cu, Kα, λ = 0.154 nm). Fourier transform infrared spectrometer (FTIR) was performed using an IR Prestige-21 spectrometer (Shimadzu, Japan) with KBr powder in the wavenumber range of 4000–500 cm^{-1}. Morphologic analysis of the sample was measured by a field emission scanning electron microscope (SEM, JEOL JSM-6700F, Japan) combined with energy-dispersive X-ray (EDX) for element mapping. Chemical states of the sample's surface elements were measured using X-ray photoelectron spectroscopy (XPS, Thermo ESCALAB 250 XI, USA). The dissolution of metal ions from MnFe-LDH was tested via an inductively coupled plasma emission spectrometer (ICP-AES, Leeman Co., Ltd., USA). Electron spin resonance (ESR) signals were detected by a JES FA200 (JEOL, Japan) spectrometer with DMPO. The total organic carbon (TOC) were determined via a Shimadzu TOC-Vwp. The residual AO7 concentration in solution was analyzed using UV–vis spectrophotometer (UV-4100 Shimadza, Japan).

The intermediate products of AO7 degradation were detected using a GC/MS-QP 2010 Plus equipped with a capillary column of DB-5 MS (30 m × 0.25 mm × 0.25 μm, Shimadzu, Japan). The samples at 5 min, 15 min and 30 min were filtered and extracted using CH_2Cl_2 for 3

times. Next, the organic phase was concentrated and injected into the GC/MS system. The GC was operated at 40 °C for 5 min, then raised to 100 °C (12 °C/min), next to 200 °C (5 °C/min), finally to 270 °C (20 °C/min) and held for 10 min. EI mode was adopted and the spectra was in a scan range of 3–500 *m/z*. The intermediates were identified using the NIST MS search 2.0 as reference.

2.4. Activity test of catalyst

Batch degradation experiments were performed to explore the influence of PMS concentration, catalyst dosage, reaction temperature, solution initial pH, initial dye concentration and anions on the AO7 degradation in MnFe-LDH/PMS system. The experiments were carried out in 250 mL reactors with constant dark stirring at room temperature. At the beginning of tests, 0.20 g/L catalysts were added dispersedly into 100 mL AO7 solution (20 mg/L) and electromagnetically stirred for 30 min to achieve adsorption-desorption dynamic equilibrium. Then a definite amount of PMS (0.20 g/L) was homogeneously dispersed into the solution to begin the catalytic degradation processes. At a certain period of time, 2.00 mL of the sample was extracted from the mixed solution, quickly filtrated using 0.22 μm membrane and monitored using the UV–vis spectrophotometer at 484.00 nm in 30 s to analyze the residual AO7 concentration. The used catalysts in the recycling experiments were gathered by centrifugal separation, washing and vacuum drying.

3. Results and discussion

3.1. Characterization of the catalyst

The composition and phase purity of LDH with different Mn/Fe molar ratios were analyzed by XRD. As shown in Fig. 1(A), the diffraction peaks at 2θ = 24.2°, 31.4°, 37.5°, 41.4°, 45.1° and 51.5° were observed, which correspond to the crystal planes of (012), (104), (110), (113), (202) and (018), respectively. The peaks of the synthesized Mn/Fe-LDH samples were in good agreement with the previous report (Kim, 2012). It can be found that the pure peaks were obtained in the prepared catalysts with the molar ratio ranging from 1 to 2. However, some impure peaks gradually appeared in the spectrum from 15.0° to 20.0° and 31.4° to 37.5° as the ratio further increasing to 4 and 8, which may suggest the formation of manganese oxide (Kim, 2012).

In order to obtain an optimum molar ratio of high crystallinity catalyst, FT-IR was also performed on these samples (Fig. 1(B)). The LDH with the Mn/Fe molar ratio at 1 and 2 almost displayed the same pattern, while these at 4 and 8 showed another same pattern, which were in accord with the XRD analysis. The broad peaks near 3421 cm^{-1} were characteristics of the stretching vibrations of hydroxyl groups in the hydroxide-like layers and the intercalated water molecules (Lu et al., 2015). Bending vibrations of the interlayers and/or adsorbed water caused the weak peaks appearing at 1633 cm^{-1} (Xie et al., 2017). The strong and sharp peaks around 1431 cm^{-1} could be assigned to the vibrational absorption of CO_3^{2-} between interlayers (Magagula et al., 2009). Besides, the peaks between 1000 and 500 cm^{-1} could be ascribed to the stretching of metal oxygen and metal hydrogen, 864 cm^{-1} was likely to be the stretching of Mn-OH, 520 cm^{-1} was Fe-OH and 725 and 607 cm^{-1} may be caused by Fe-O and Mn-O, respectively (Abdelkader et al., 2011; Gong et al., 2017; Lu et al., 2015; Magagula et al., 2009).

The SEM images and EDS spectrum of the prepared MnFe-LDH (1:1) are depicted in Fig. 1(C–D). Samples were found to be agglomerated and rounded from Fig. 1(C), which was consistent with previous report (Kim, 2012). Moreover, the peaks of EDS spectrum showed that the atomic percent elements of C, O, Mn and Fe were 15.86%, 57.29%, 12.40% and 11.36% (Fig. 1(D)), respectively. And the calculated molar ratio of Mn/Fe was 1.09, in good agreement with the initial molar ratio.

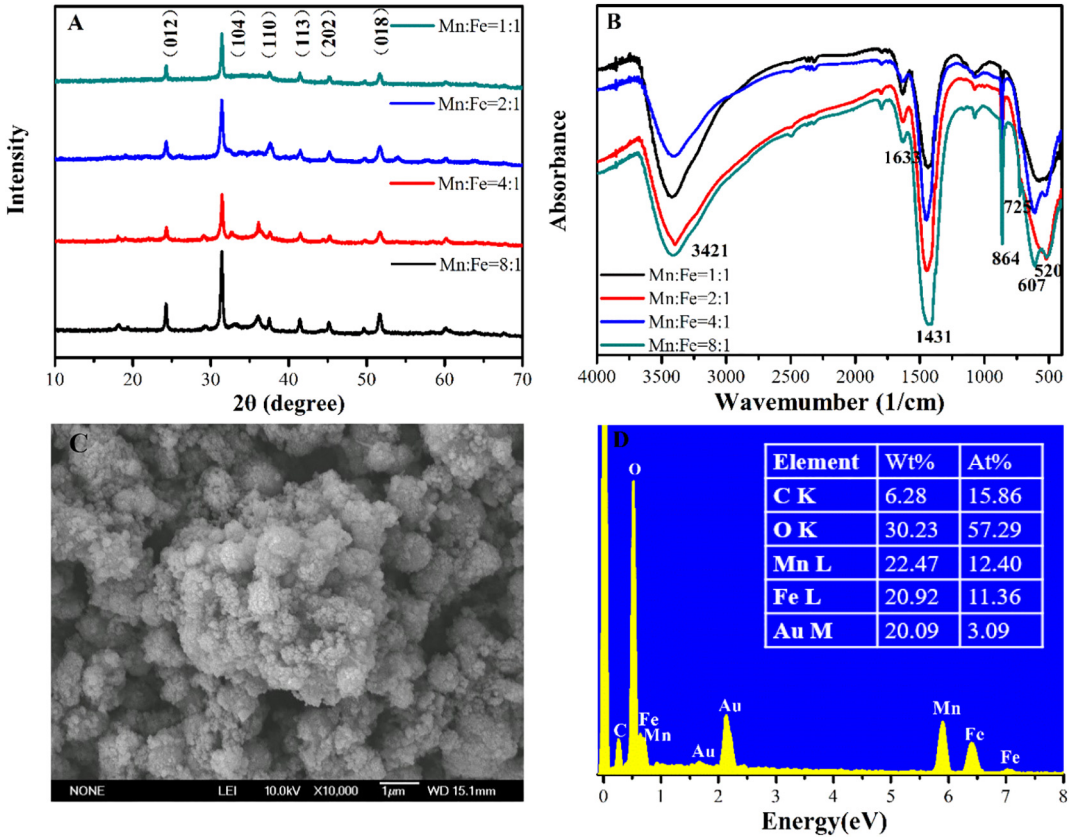

Fig. 1. Representative XRD spectra (A) and FTIR spectra (B) of MnFe-LDH with different Mn/Fe molar ratios; SEM image (C) and EDS analysis (D) of MnFe-LDH.

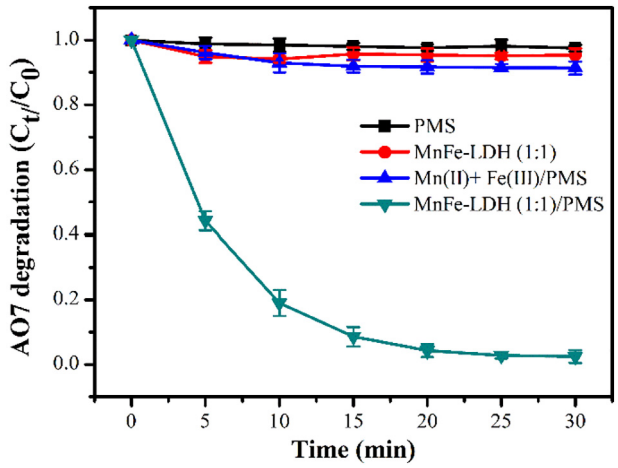

Fig. 2. AO7 removal in different systems. Reaction conditions: initial AO7 concentration = 20 mg/L, catalyst dosage = 0.20 g/L, PMS concentration = 0.20 g/L, solution pH = 6.10 and reaction temperature = 25 °C.

3.2. Catalytic activity of LDH

Fig. 2 shows the AO7 degradation in various systems, including PMS and Mn(II) + Fe(III)/PMS systems, as well as heterogeneous MnFe-LDH (1:1) and MnFe-LDH (1:1)/PMS systems. Under PMS oxidation alone, nearly no significant AO7 degradation was noticed. Besides, the adsorption of AO7 on MnFe-LDH (1:1) was stable at 4.60% after 30 min, suggesting that the adsorption of AO7 was negligible in the MnFe-LDH and MnFe-LDH/PMS systems. However, an excellent degradation of AO7 was achieved in the MnFe-LDH(1:1)/PMS system, and 97.56% of AO7 was degraded within 30 min. Comparably, the degradation efficiency of AO7 in Mn(II) + Fe(III)/PMS system with the same metal amount of the MnFe-LDH(1:1) was only 8.64%. These results indicated that MnFe-LDH was likely to be an efficient activator of PMS for destroying the structure of AO7 and enhancing the AO7 degradation.

To determine the best molar ratio for the as-prepared samples, the catalysts with different Mn/Fe molar ratio were all used to active PMS for degrading AO7. As shown in Fig. 3(A), the degradation efficiency of AO7 increased firstly and then decreased with the increase of Mn/Fe molar ratio. The obtained activators of MnFe-LDH(1:1) and MnFe-LDH (2:1) exhibited the optimal AO7 removal efficiencies, reaching to 97.56% and 97.29% within 30 min, respectively. Besides, the corresponding kinetic curves of different Mn/Fe molar ratios in MnFe-LDH/PMS systems are showed in Fig. 3(B). The process followed the pseudo-first-order kinetic well. As the molar ratio serially increased, the k increased firstly from 0.0341 to 0.1419 min^{-1} but then decreased to 0.0121 min^{-1} (Table 1). The results demonstrated that the efficiency of Mn(II) for the PMS activation was higher than that of Fe(III) (Ghanbari and Moradi, 2017; Zhao et al., 2018). However, when Mn/Fe molar ratio was higher than 2, the reversible redox process of Mn and Fe were negatively affected, causing poor activation of PMS and low degradation of AO7. Hence, considering the excellent catalytic degradation efficiency and high kinetic constant, MnFe-LDH (1:1) was selected to be an optimal activator for PMS heterogeneous activation.

3.3. Influence of AO7 degradation parameters

3.3.1. Influence of PMS concentration and catalyst dosage

The decolorization of AO7 over MnFe-LDH/PMS was further investigated at different concentrations of PMS (Fig. 4(A–B)). It was obvious that the removal efficiency and rate of AO7 were gradually improved as the PMS concentration increased from 0.05 to 0.20 g/L. However, no significant improvement in AO7 degradation was observed as PMS concentration further raised to 0.80 g/L. The results revealed that increasing the concentration of PMS was useful to promote the AO7 removal, but the excessive has little effect. Because the moderate PMS concentration favored the productions of active radicals, which destroy the chromophoric groups and degrade the dye (Gong et al., 2017). However, the redundant PMS in solution can react with $SO_4^{\bullet -}$ and •OH to produce $SO_5^{\bullet -}$, which is a weaker oxidant with redox potential of 1.1 V, resulting in worse degradation of AO7 (Eqs. (1) and (2)) (Ahmadi and Ghanbari, 2018; Gong et al., 2017).

$$HSO_5^- + SO_4^{\cdot -} \rightarrow SO_5^{\cdot -} + SO_4^{2-} + H^+ \quad (1)$$

$$HSO_5^- + {}^{\cdot}OH \rightarrow SO_5^{\cdot -} + H_2O \quad (2)$$

Fig. 4(C–D) showed the influence of catalyst dosage on AO7 degradation. Obviously, the AO7 removal efficiency and rate serially increased with adding catalysts. When the amount of catalysts increased from 0.05 to 0.20 g/L, the corresponding discoloration rate increased from 51.89% to 97.56%. Actually, more catalysts provide more active sites and active radicals for the PMS activation, further enhancing the degradation of AO7. However, overlapped curves showed that the improvement of AO7 degradation was little as the concentration of catalyst increased to 0.80 g/L.

3.3.2. Influence of reaction temperature and solution initial pH

As seen from Fig. 5(A–B), higher reaction temperature could enhance the rate of AO7 degradation using MnFe-LDH as catalyst. Specifically, the AO7 removal efficiency could reach 97.00% in a short time

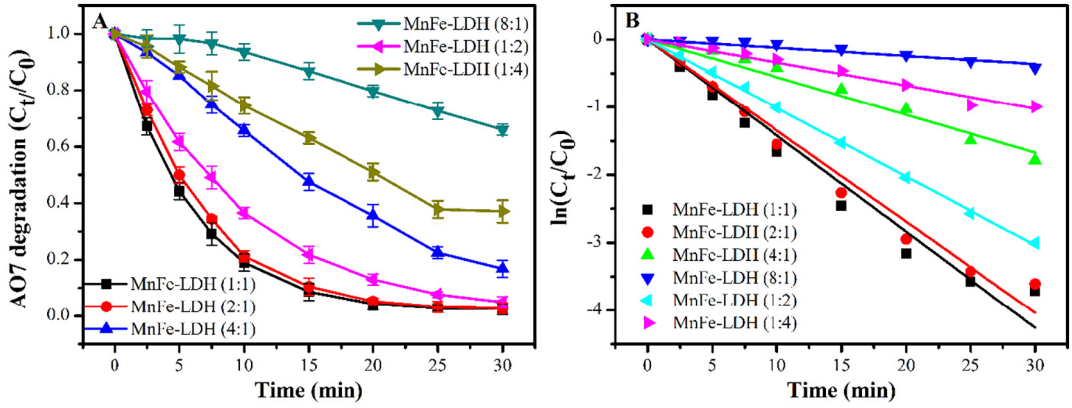

Fig. 3. Degradation of AO7 (A) and kinetic curves (B) of different Mn/Fe molar ratios. Reaction conditions: initial AO7 concentration = 20 mg/L, catalyst dosage = 0.20 g/L, PMS concentration = 0.20 g/L, solution pH = 6.10 and reaction temperature = 25 °C.

Table 1
Pseudo-first-order rate constants (k) of AO7 degradation under different Mn/Fe molar ratios in MnFe-LDH/PMS system.

LDH-sample	$\ln(C_t/C_0) = -kt$. (pseudo-first-order kinetic)		
	$k(min^{-1})$	R^2	Standard error
MnFe-LDH(1:4)	0.03	0.99	0.0012
MnFe-LDH(1:2)	0.10	1.00	0.0005
MnFe-LDH(1:1)	0.14	0.99	0.0057
MnFe-LDH(2:1)	0.13	0.99	0.0044
MnFe-LDH(4:1)	0.06	0.99	0.0022
MnFe-LDH(8:1)	0.01	0.96	0.0008

(25 min) at room temperature (about 25 °C). Further increasing the temperature to 35 °C, and 45 °C (even 55 °C), the degradation time reached to the same removal rate was shorted to 20 min and 15 min, respectively. The corresponding reaction rate constants were formulated by the pseudo-first-order kinetic and presented at Table 2. The results indicated that the organic pollutant removal in MnFe-LDH/PMS system was an endothermic reaction. The activation energy was calculated to be 21.32 kJ/mol based on Arrhenius equation (Eq. (3)).

$$\ln(k) = \frac{E_a}{R}\frac{1}{T} + \ln(A) \quad (3)$$

Fig. 6(A–B) presented that solution initial pH played a crucial role on AO7 degradation in MnFe-LDH/PMS system. The highest degradation rate of AO7 (97.93%) was achieved at neutral pH (7.0). Meanwhile, there was a comparative degradation efficiency (97.56%) at blank pH (6.1) to neutral pH (7.0), indicating that MnFe-LDH could better activate PMS under neutral condition. And there was no obvious variation for AO7 degradation with pH ranging from 5.0 to 9.0. Nevertheless, the degradation efficiency decreased to 75.15% at pH 11.0. In alkaline solution (pH = 11.0), PMS was mainly decomposed to SO_5^{2-} in the non-radical pathway for the solution pH was higher than the pKa of PMS (9.4), resulting in reduced free radicals and decreased degradation of AO7 (Ahmadi and Ghanbari, 2018; Hu et al., 2017). In acidic conditions (pH = 3.0), more leaching of Mn and Fe from the catalyst could be observed, resulting in less active sites of PMS activation and a loss of catalytic capacity of the catalyst, and decreasing the degradation efficiency to 41.13%. Although the homogeneous reaction between leached metal and PMS could also lead to AO7 degradation, the degradation efficiency was much lower than that of MnFe-LDH/PMS system (Fig. 3). Meanwhile, the reduction of degradation efficiency could also be attributed to excessive amounts of H^+, which could scavenge $SO_4^{\bullet -}$ and •OH according to Eqs. (4) and (5), respectively (Ahmadi and Ghanbari, 2018; Huang et al., 2009; Mohammad Ali Zazouli et al., 2017).

$$H^+ + SO_4^{\cdot -} + e^- \rightarrow HSO_4^- + SO_4^{2-} \quad (4)$$

$$H^+ + {}^{\cdot}OH + e^- \rightarrow H_2O \quad (5)$$

Leaching of Mn and Fe during reactions at different initial solution pH were shown in Fig. 6(C–D). The lower the initial pH of the solution, the more the initial leaching amount of metal. At the initial pH of 3, the initial leaching amount of Mn and Fe reached the maximum of 4.49 and 0.11 mg/L, respectively. The leaching of Mn and Fe was very few when the initial pH of AO7 solution ranged from 5.0 to 11.0. However, the amount of metal leaching first increased and then decreased with the reaction proceeding. The increase of metal leaching was mainly due to the addition of PMS, which decreased the pH of the solution. And the decrease of metal leaching might be on account of the adsorption of MnFe-LDH.

Fig. 6(E) showed the variation of pH during the reactions. In the adsorption stage, the pH of the solution changed slightly due to the buffer effect of the catalyst. When the initial pH was ranged from 3.0 to 9.0, pH showed a final decrease to 2.7–3.9 along with the degradation process.

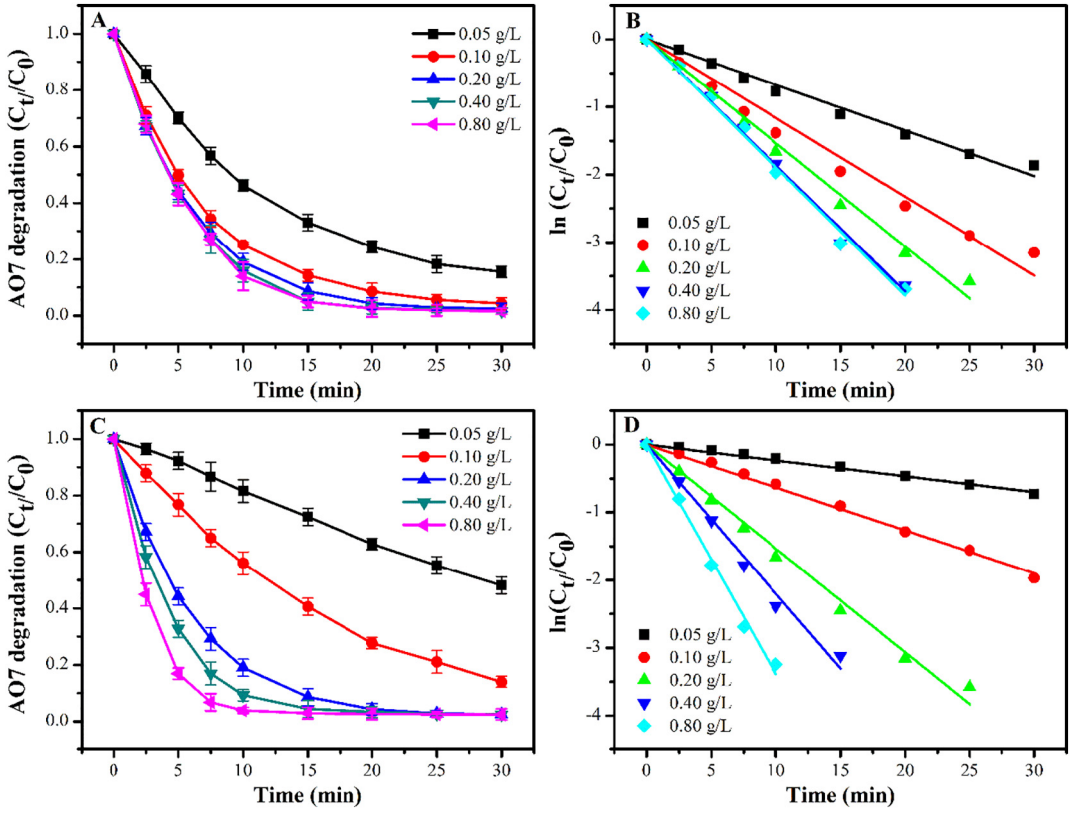

Fig. 4. Influence of PMS concentration (A) and kinetic curves (B) on AO7 degradation; influence of catalyst dosage (C) and kinetic curves (D) on AO7 degradation. Reaction conditions: initial AO7 concentration = 20 mg/L, catalyst dosage = 0.20 g/L, PMS concentration = 0.20 g/L, solution pH = 6.10 and reaction temperature = 25 °C.

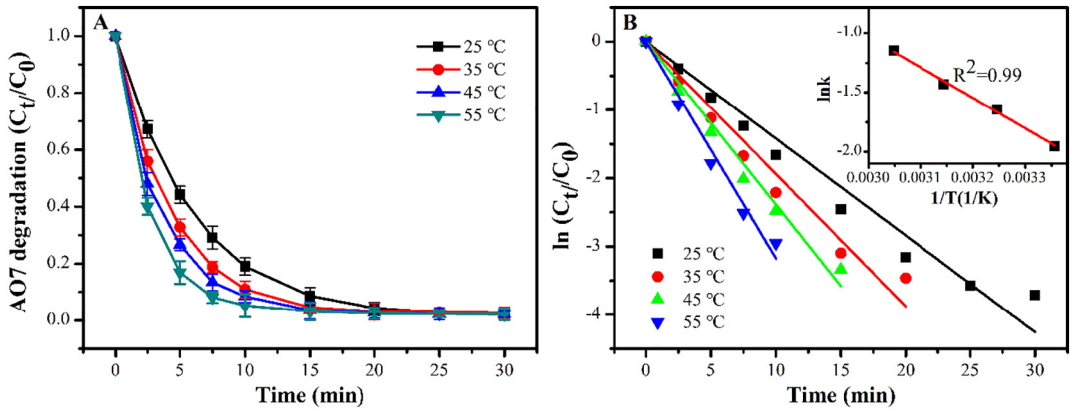

Fig. 5. Influence of reaction temperature (A) and kinetic curves (B) on AO7 degradation. Reaction conditions: initial AO7 concentration = 20 mg/L, catalyst dosage = 0.20 g/L, PMS concentration = 0.20 g/L and solution pH = 6.10.

When the initial pH was at 11.0, the pH decreased to 7.1. The decrease of pH during the oxidation processes of activated PMS has been observed (Du et al., 2016; Yao et al., 2013). The decrease of pH was attributed to the catalytic decomposition of PMS, the formation of acidic intermediates, the buffer effect of catalyst and the oxidation of water molecules by sulfate radicals produced by PMS activation (Du et al., 2016; Yao et al., 2013).

3.3.3. Influence of initial AO7 concentration

Fig. 7(A–B) showed that both the AO7 degradation rate and efficiency decreased as the AO7 concentration increasing from 10 to 100 mg/L. The higher the initial AO7 concentration in the solution, the more the time to reach the same degradation efficiency. When the AO7 concentrations were lower and at 10, 20 and 40 mg/L, the corresponding time to reach the degradation efficiency >95.00% was 20, 30 and 40 min, respectively. While under same reaction conditions, in order to the same efficiency, it took about >60 min and 120 min at higher AO7 concentrations of 60 and 100 mg/L, respectively. The AO7 degradation rate was up to 0.16 min^{-1} at AO7 concentration of 10 mg/L, while only 0.02 min^{-1} at 100 mg/L. In fact, when the initial dye concentration increased, the reactive radicals provided by a certain amount of PMS became inadequate, thus lowering the degradation efficiency.

3.3.4. Influence of anions during AO7 degradation process

It is well known that versatile anions can react rapidly with the generated living radicals, further affect the catalytic degradation process. In practical wastewater, there are plenty of inorganic anions such as Cl^-, CO_3^{2-}, and NO_3^-, which maybe significantly influence the degradation of organic pollutants by sulfate radical-based AOPs. In this study, the influences of anions including Cl^-, CO_3^{2-}, and NO_3^- (0.1 mol/L) were investigated and the results are illustrated in Fig. 8(A–B). The existence of Cl^- significantly enhanced the degradation rate and efficiency of AO7, which could be ascribed to the reaction of Cl^- with HSO_5^- to generate Cl_2 and HOCl (Eqs. (6) and (7)) (Ahmadi et al., 2017; Ruixia Yuan et al., 2011). Previous researches demonstrated that Cl_2 and HOCl produced had a good effect for the dye bleaching (Ahmadi et al., 2017). Similar phenomenon also was observed in AO7 decolorization by Co/PMS (Ruixia Yuan et al., 2011). The NO_3^- anions had slight inhibitory effects on AO7 degradation, as NO_3^- anions could scavenge sulfate and hydroxyl radicals and produce nitrate radicals with lower redox potential of 2.3–2.7 V (Ahmadi and Ghanbari, 2019; Jiang et al., 1992). However, the degradation efficiency and rate of AO7 greatly declined in the presence of CO_3^{2-}. There are three mechanisms to explain the negative influence. Firstly, CO_3^{2-}, as an alkaline ion, could increase the pH of AO7 solution from 6.1 to 11.5 based on Eq. (8). Secondly, the CO_3^{2-} and HCO_3^- produced could react with free radicals at a high rate constant of 10^6–10^8 M^{-1} s^{-1} to produce $CO_3^{\bullet-}$ and $HCO_3^{\bullet}$ respectively, which are weaker oxidants compared to sulfate and hydroxyl radicals (Dhaka et al., 2018). Finally, the HCO_3^- may react directly with HSO_5^- to produce HCO_4^- (Eq. (9)) (Ahmadi and Ghanbari, 2019).

$$Cl^- + HSO_5^- \rightarrow SO_4^{2-} + HOCl \quad (6)$$

$$2Cl^- + HSO_5^- + H^+ \rightarrow Fe^{3+} + SO_4^{2-} + Cl_2 + H_2O \quad (7)$$

$$CO_3^{2-} + H_2O \rightarrow HCO_3^- + OH^- \quad (8)$$

$$HSO_5^- + HCO_3^- \rightarrow HSO_4^- + HCO_4^- \quad (9)$$

3.4. Plausible mechanism

To determine the vital active free radicals for the AO7 degradation in MnFe-LDH/PMS system, quenching tests using methanol (MA), tertiary butanol (TBA) and phenol as quenching agent were carried out. It is well-known that MA, TBA and phenol possess high reactivities with hydroxyl radicals and the reaction rates are 9.7×10^8, $(3.8–7.6) \times 10^8$ and 6.6×10^9 M^{-1} s^{-1}, respectively (Chen et al., 2016; Zhang et al., 2013). However, phenol have a higher reactivity with sulfate radical ($k_{SO4\bullet-}$: 8.8×10^9 M^{-1} s^{-1}) than MA and TBA ($k_{SO4\bullet-/MA}$: 3.2×10^6 M^{-1} s^{-1}; $k_{SO4\bullet-/TBA}$: $(4.0–9.1) \times 10^5$ M^{-1} s^{-1}) (Chen et al., 2016; Zhang et al., 2013). Fig. 9(A) showed that 97.56% of AO7 was degraded without quenching agent in the LDH/PMS system, while 94.93%, 82.97% and 22.33% of AO7 were degraded with the quenching agent of MA, TBA and phenol, respectively. It suggested that MA, TBA and phenol had the inhibiting effects on AO7 degradation, ascribing to the competing consumption of radical scavengers by •OH and $SO_4^{\bullet-}$ (Huang et al., 2017). Nevertheless, the inhibition of TBA was always more significant than that of MA, which have been reported by other authors (Dong et al., 2016; Huang et al., 2017; Zhang et al., 2013). This result may be attributed to the fact that the surface of MnFe-LDH had a stronger affinity for AO7 than MA and its masking effect on the bonding sites can be dispersed by TBA, which was due to its adsorption at a high concentration (Dong et al., 2016; Huang et al., 2017). But the inhibition of AO7 degradation led by the addition of phenol was more notedly than that resulted by MA and TBA. Thus, $SO_4^{\bullet-}$ and •OH all played the dominant roles in AO7 removal of the LDH/PMS system (Hu et al., 2019).

Table 2
Experimental results of AO7 degradation at different temperatures.

T(°C)	k(min^{-1})	R^2 of k	Standard error	Ea(kJ/mol)	R^2 of ΔE
25	0.14	0.99	0.0057	21.32	0.99
35	0.19	0.99	0.0086		
45	0.24	0.99	0.0086		
55	0.32	0.99	0.0126		

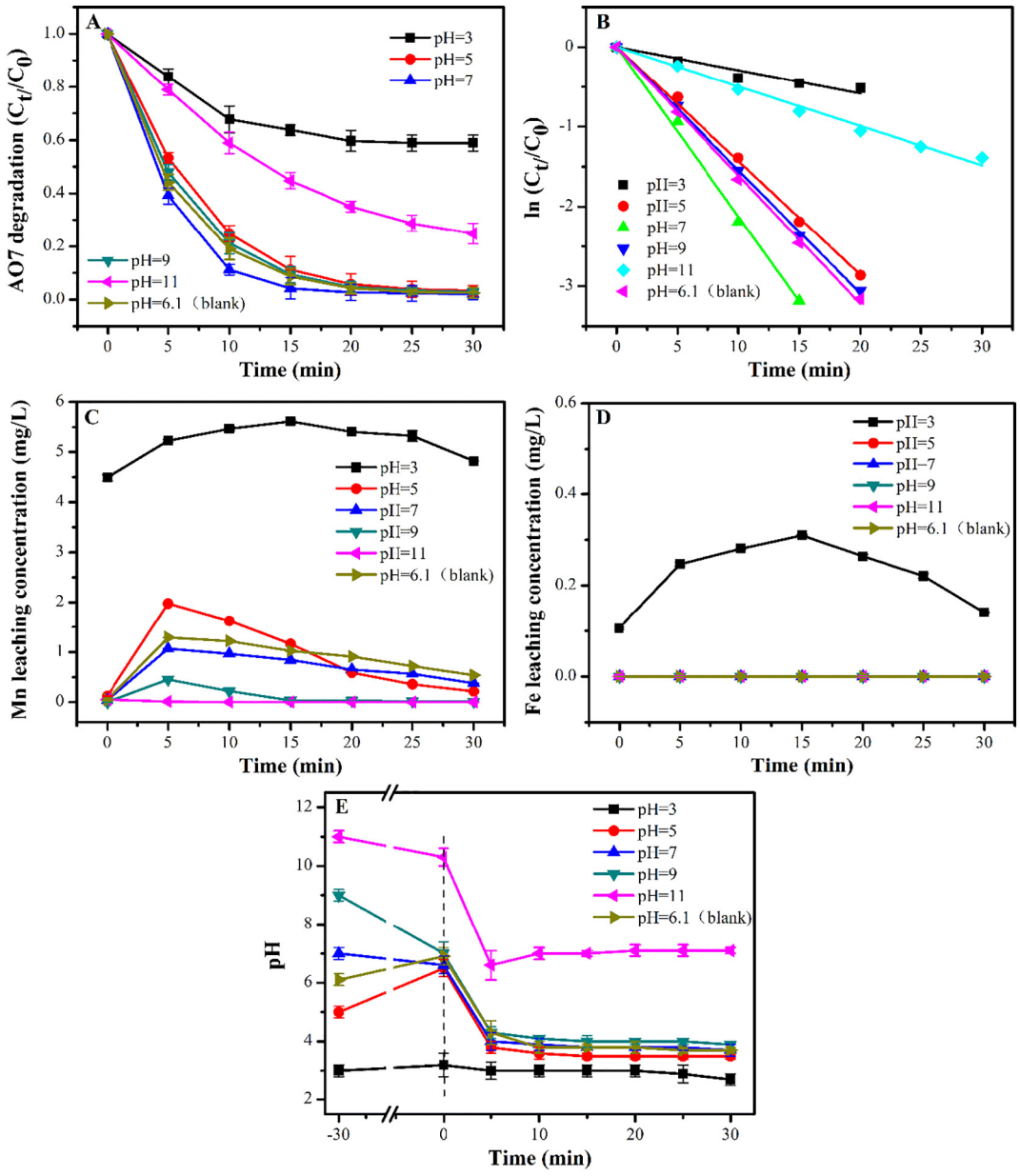

Fig. 6. Influence of solution initial pH(A) and kinetic curves (B) on AO7 degradation; leaching of Mn (C) and Fe (D) during reactions at different initial pH values; the pH variation (E) in MnFe-LDH/PMS system. Reaction conditions: initial AO7 concentration = 20 mg/L, catalyst dosage = 0.20 g/L, PMS concentration = 0.20 g/L and reaction temperature = 25 °C.

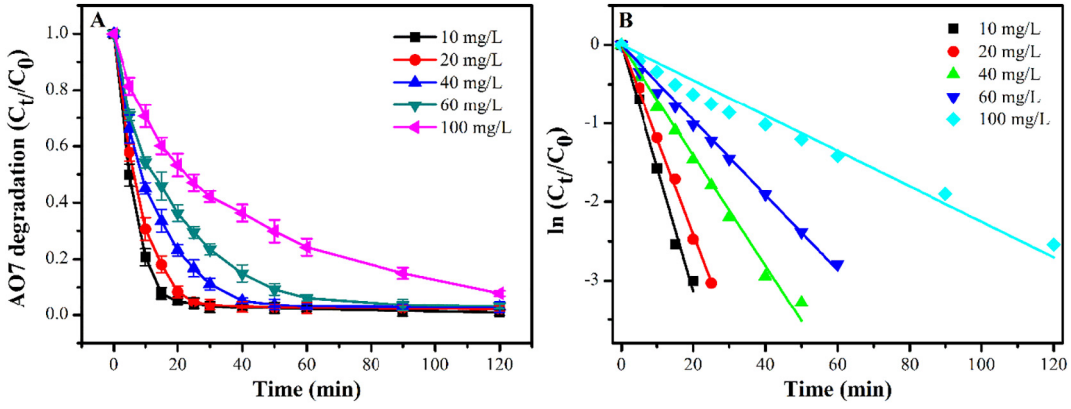

Fig. 7. Influence of initial AO7 concentration (A) and kinetic curves (B) on AO7 degradation. Reaction conditions: catalyst dosage = 0.20 g/L, PMS concentration = 0.20 g/L, solution pH = 6.10 and reaction temperature = 25 °C.

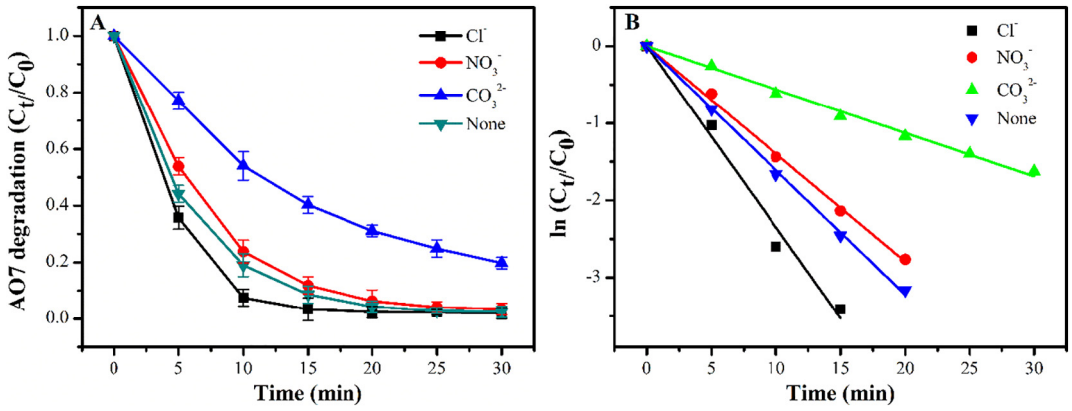

Fig. 8. Influence of anions (A) and kinetic curves (B) on AO7 degradation. Reaction conditions: initial AO7 concentration = 20 mg/L, catalyst dosage = 0.20 g/L, PMS concentration = 0.20 g/L, solution pH = 6.10, reaction temperature = 25 °C and anions dose = 0.10 mol/L.

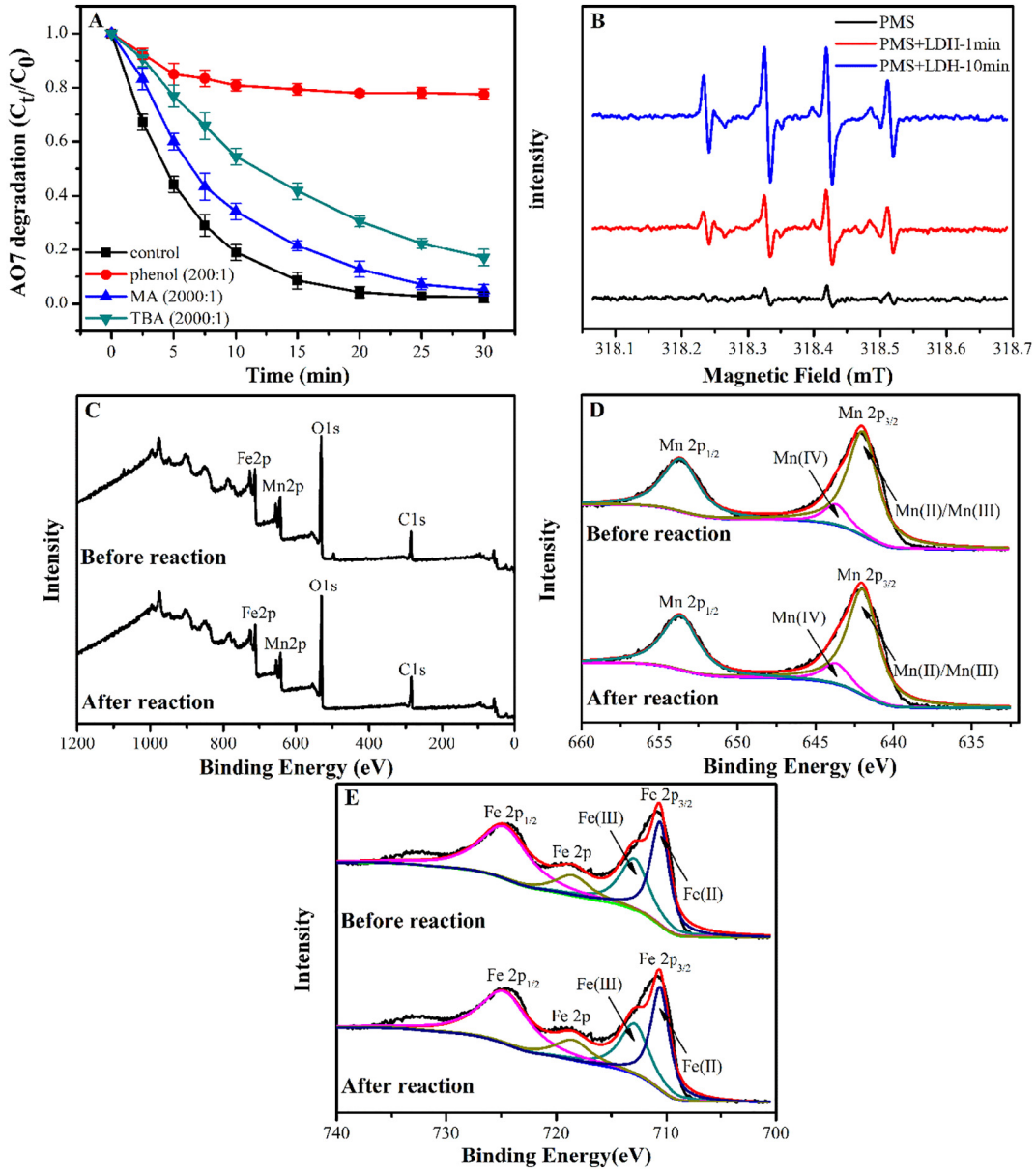

Fig. 9. AO7 degradation in the presence of different radical scavengers (A), EPR spectra (B), survey XPS spectrum (C), Fe 2p XPS spectra (D) and Mn 2p XPS spectra (E) of MnFe-LDH before and after reaction. Reaction conditions: initial AO7 concentration = 20 mg/L, catalyst dosage = 0.20 g/L, PMS concentration = 0.20 g/L, solution pH = 6.10 and reaction temperature = 25 °C.

To further confirm the generations of sulfate radicals in the MnFe-LDH/PMS system, the EPR test using DMPO as a spin trapping agent was conducted (Fig. 9(B)). Only small peaks were acquired in the PMS solutions, which were assigned to DMPO-•OH ($\alpha_H = 1.47$ mT, $\alpha_N = 1.50$ mT), indicating that little hydroxyl could be produced by PMS in the absence of catalyst (Yang et al., 2017). When MnFe-LDH was added to the PMS solution, a series of peaks that could assign the characteristic signals to DMPO-•OH ($\alpha_H = 1.47$ mT, $\alpha_N = 1.50$ mT) and DMPO-SO_4•$^-$ ($\alpha_H = 0.08$ mT, $\alpha_H = 0.15$ mT, $\alpha_H = 1.02$ mT, $\alpha_N = 1.37$ mT) were observed, which were consistent with the reports of Wei et al. and Hu et al. (Hu et al., 2019; Wei et al., 2017). Above results fully confirmed that hydroxyl radicals and sulfate radicals were generated in the system. The peak strength of DMPO-•OH increased remarkably compared with the PMS solutions without MnFe-LDH at 1 min. Further extended the time to 10 min, the intensity of DMPO-•OH signal increased rapidly, while the strength of DMPO-SO_4•$^-$ signal showed little or no increase. The above results indicated that PMS could be activated by MnFe-LDH to produce •OH and SO_4•$^-$ and the generated SO_4•$^-$ can react to produce more •OH (Gong et al., 2017; Wang et al., 2015). Thus, Mn and Fe with variable valence in MnFe-LDH might have played important roles in the activation of PMS.

XPS measurement was employed to analyze the valence changes of Mn and Fe in the MnFe-LDH/PMS system before and after reaction (Fig. 9(C–E)). As depicted in Fig. 9(C), the full survey scan spectra of MnFe-LDH before and after reaction showed no obvious changes, which confirmed the excellent stability of MnFe-LDH. In particular, the binding energy values for Mn $2p_{1/2}$ and Mn $2p_{3/2}$ declined from 653.68 and 642.18 eV to 653.88 and 642.08 eV after reaction, respectively (Fig. 9(D)) (Su et al., 2019; Zhao et al., 2018). The proportion of Mn(IV) varied little, which inferred that the valence changes of Mn mainly occurred in Mn(II)/Mn(III). From Fig. 9(E), Fe 2p was resolved into two peaks at 711.18 eV and 723.98 eV, corresponding to the shake-up satellite peaks of Fe $2p_{3/2}$ and Fe $2p_{1/2}$, implying that the iron in the fresh materials was mainly in the state of Fe(III) (Gong et al., 2017b). However, these peaks slightly shifted and the peak area of Fe(III) decreased after the reaction. It was found that 22.02% Fe(III) was transformed to Fe(II). These results indicated that Mn(II)/Mn(III) and Fe(III)/Fe(II) can be mutually transformed into each other in the MnFe-LDH/PMS system.

According to the results of EPR, quenching tests and XPS measurement, the main degradation processes for AO7 were proposed as follows. On the basis of the XPS analysis spectrum, Mn(II), Mn(III), Fe(II) and Fe(III) may be involved in the reaction. At first, both Mn(II) and Fe(II) of the surface of MnFe-LDH activated PMS to generate surface-bound •OH and SO_4•$^-$ by donating electrons and to produce Mn(III) and Fe(III) sites (Eqs. (10)–(13)) (Huang et al., 2017; Xie et al., 2017; Yang et al., 2015a). Then, the produced Mn(III) and Fe(III) sites reactivated PMS to generate SO_5•$^-$ through getting electrons and to produce Mn(II) and Fe(II) sites, forming the circulations of Mn and Fe (Eqs. (14)–(15)) (Huang et al., 2017). The redox cycles of Mn and Fe were combined together by the reaction between Mn(III) and Fe(II). Besides, the metals of Mn and Fe can be oxidized and reduced reversibly based on the especial octahedral structure of the LDHs (Eq. (18)). It was believed that the transformation between Mn(III) and Fe(II) was thermodynamically advantageous on account of the normal reduction potential of metals (Gong et al., 2017; Huang et al., 2017). Since the standard redox potential of Mn(III)/Mn(II) (1.51 V) is higher than that of Fe(III)/Fe(II) (0.77 V), the Fe(II) sites may give an electron to the Mn(III) sites and transform into Fe(III) and Mn(II) sites (Eqs. (16)–(17)). The regeneration of the active sites of MnFe-LDH made the activation cycle go on until the PMS was completely consumed. The generated SO_5•$^-$ and SO_4•$^-$ can react with OH^- to produce •OH (Eqs. (19) and (20)) (Huang et al., 2017; Wang et al., 2015). Besides, •OH was also generated by the reaction with SO_4•$^-$ and H_2O (Eq. (21)) (Yang et al., 2015a; Zhao et al., 2018). At last, the generated strong oxidation of SO_4•$^-$ and •OH oxidized AO7 to generate various intermediate degradation products and decomposed into $C_nH_{2n-1}COOH$ (Eq. (22)) (Yang et al., 2015c). The excellent catalytic activity of MnFe-LDH may be related to the positive synergistic effect between Mn and Fe. The redox reaction between Mn and Fe accelerated electron transfer and recovered the MnFe-LDH, which enhanced the activity of PMS to produce SO_4•$^-$ and •OH, the efficiency of degradation of organic pollutants and the reusability.

$$\equiv Mn^{2+} + HSO_5^- \rightarrow \equiv Mn^{3+} + SO_4^{2-} + {}^{\cdot}OH \quad (10)$$

$$\equiv Fe^{2+} + HSO_5^- \rightarrow \equiv Fe^{3+} + SO_4^{2-} + {}^{\cdot}OH \quad (11)$$

$$\equiv Mn^{2+} + HSO_5^- \rightarrow \equiv Mn^{3+} + SO_4{}^{\cdot -} + OH^- \quad (12)$$

$$\equiv Fe^{2+} + HSO_5^- \rightarrow \equiv Fe^{3+} + SO_4{}^{\cdot -} + OH^- \quad (13)$$

$$\equiv Mn^{3+} + HSO_5^- \rightarrow \equiv Mn^{2+} + SO_5{}^{\cdot -} + H^+ \quad (14)$$

$$\equiv Fe^{3+} + HSO_5^- \rightarrow \equiv Fe^{2+} + SO_5{}^{\cdot -} + H^+ \quad (15)$$

$$\equiv Mn^{3+} + e^- \rightarrow Mn^{2+}, E^0 = 1.51V \quad (16)$$

$$\equiv Fe^{3+} + e^- \rightarrow \equiv Fe^{2+}, E^0 = 0.77V \quad (17)$$

$$\equiv Mn^{3+} + \equiv Fe^{2+} \rightarrow \equiv Mn^{2+} + \equiv Fe^{3+} \quad (18)$$

$$2SO_5{}^{\cdot -} + 2OH^- \rightarrow 2SO_4^{2-} + 2{}^{\cdot}OH + O_2 \quad (19)$$

$$SO_4{}^{\cdot -} + OH^- \rightarrow SO_4^{2-} + {}^{\cdot}OH \quad (20)$$

$$SO_4{}^{\cdot -} + H_2O \rightarrow SO_4^{2-} + {}^{\cdot}OH + H^+ \quad (21)$$

$$SO_4{}^{\cdot -}/{}^{\cdot}OH + AO7 \rightarrow CnH2n-1COOH + SO_4^{2-} \quad (22)$$

3.5. Degradation pathways

To find out the temporal evolution of AO7 molecular structure characteristics in the degradation of MnFe-LDH/PMS system, samples were taken at a given interval and detected by UV–vis spectra. The UV–vis spectrum (Fig. 10) showed five characteristic peaks at 228, 251, 309, 422 and 484 nm, all of which related to different substances. The typical peaks at 484 nm was ascribed to the azo linkage of AO7 in the form of hydrazine, and other peaks were attributed to the azo linkage of AO7

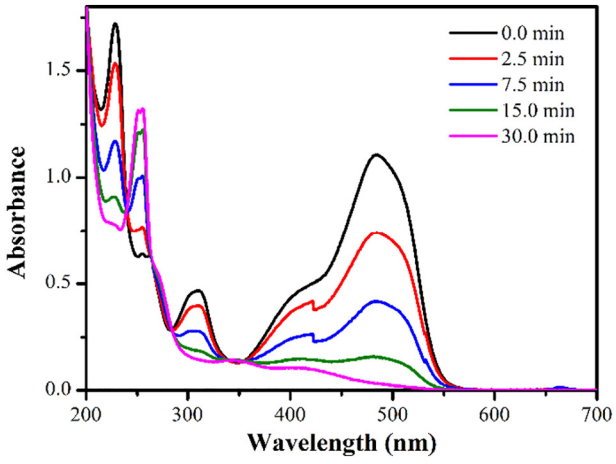

Fig. 10. UV–vis spectra of AO7 degradation at different times in MnFe-LDH/PMS system. Reaction conditions: initial AO7 concentration = 20 mg/L, catalyst dosage = 0.20 g/L, PMS concentration = 0.20 g/L, solution pH = 6.10 and reaction temperature = 25 °C.

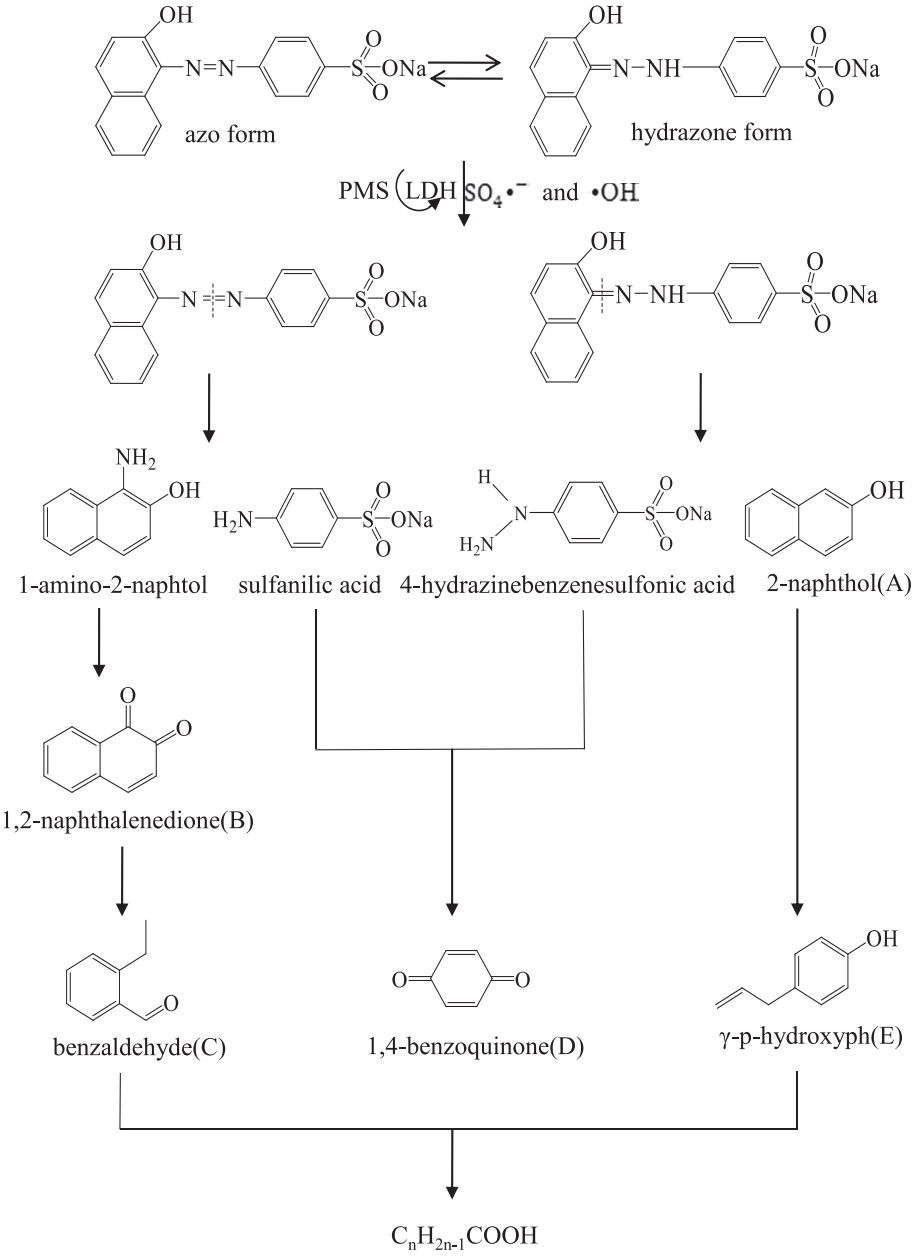

Fig. 11. Degradation pathways of AO7 in MnFe-LDH/PMS system.

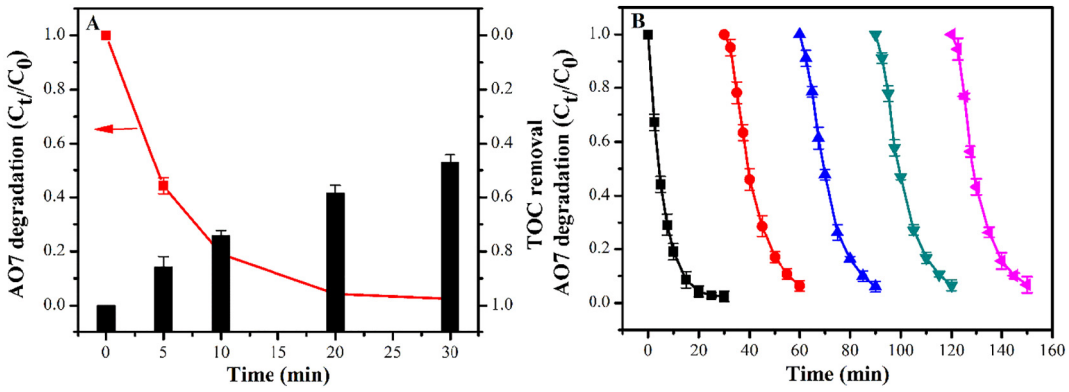

Fig. 12. TOC removal and AO7 degradation (A) and AO7 degradation using reusable MnFe-LDH (B) in MnFe-LDH/PMS system. Reaction conditions: initial AO7 concentration = 20 mg/L, catalyst dosage = 0.20 g/L, PMS concentration = 0.20 g/L, solution pH = 6.10 and reaction temperature = 25 °C.

in the azo form (Yang et al., 2015c). Furthermore, the other two peaks located at 228 and 309 nm were mainly caused by naphthalene and benzene rings, respectively (Azam and Hamid, 2006; Zhang et al., 2006). And the peaks at 251 nm might be attributed to the intermediate products (Chen et al., 2014; Qi et al., 2016). With the process of reaction, the visible peaks significantly lowered at the same time and the AO7 solution faded, which can be attributed to the fragmentations of azo linkages of AO7 (Hammami et al., 2008). Besides, the reduced peaks of naphthalene and benzene rings suggested that the aromatic fragments of AO7 and its partial intermediates were degraded and produced the peaks of the non-degradable intermediate products at 251 nm in the system. Finally, after the degradation for 30 min, the characteristic peaks of AO7 disappeared and AO7 solution became colorless.

To further investigate the pathways of AO7 degradation in MnFe-LDH/PMS system, GC–MS and NIST date comparisons were used to identify the main intermediate degradation products. Five kinds of aliphatic products (A-E) were detected (Table S1.). The potential degradation pathways of AO7 (Fig. 11) could be obtained according to these results and previous studies. Specifically, N═N bond of AO7 in the azo form was cleaved by the active $SO_4^{\bullet-}$ and •OH to produce sulfanilic acid and 1-amino-2-naphtolin, which was the primary part of AO7 degradation (Zhao et al., 2010). Furthermore, the active radical species also attacked C═N bond of AO7 in the form of hydrozone, producing 2-naphthol(A) and 4-hydrazinebenzenesulfonic acid (Hammami et al., 2008). But the GC–MS didn't detect some products due to the good solubility of 4-hydrazinebenzenesulfonic acid and sulfanilic acid and the oxidability of 1-amino-2-naphtol in air (Michael Kudlich et al., 2009). Further oxidation from the 1-amino-2-naphtoltakes placed and formed 1,2-naphthalenedione(B), then it was oxidized by $SO_4^{\bullet-}$ and •OH to lead the formation of benzaldehyde(C). At the same time, 2-naphthol was oxidized to generate γ-p-hydroxyph(E) and 4-hydrazinebenzenesulfonic acid β-naphtalenol(A). Besides, the further oxidation of desulfurization led sulfanilic acid and 4-hydrazinebenzenesulfonic acid to form 1,4-benzoquinone(D) by $SO_4^{\bullet-}$ and •OH (Guo et al., 2016). Finally, these main intermediate products were further degraded into the smaller molecule compounds.

3.6. Mineralization study

During oxidation processes, AO7 molecular may be converted into some small compounds. To determine the mineralization of AO7, TOC analysis was conducted and the results are illustrated in Fig. 12(A). With the reaction time increasing, the mineralization of AO7 in MnFe LDH/PMS system gradually increased and the 52.91% of TOC removal rate was gained after 30 min reaction. Meanwhile, the decolorization rate of AO7 reached 97.56% within 30 min, indicating that MnFe LDH had a good catalytic performance for the decolorization of AO7. During the degradation process, the AO7 firstly decomposed into intermediate products, small molecular compounds. Finally, the partial small compounds were degraded into CO_2 and H_2O. The pathway of AO7 degradation is shown in Fig. 11.

3.7. Reusability and stability of the catalysts

The recyclability and stability of catalyst were important factors for the practical application in economic perspective. After each reaction, the solution was centrifuged to collect the catalyst. Then, the collected catalyst was washed four times with absolute ethanol and deionized water. Next, the catalyst was dried in a vacuum oven at 60 °C for 24 h. Finally, 0.20 g/L reused catalyst was used again for the degradation of AO7. The ratio of reused catalyst after each reaction was 95.00%. Corresponding results was presented in Fig. 12(B). In the second run, the degradation efficiency showed a slight decrease compared with the first run, decreased from 97.56% to 93.73%, which could be put down to the adsorption of AO7 on the catalyst surface (Saputra et al., 2014; Wang et al., 2017). However, the degradation efficiency of AO7 was quite stable in subsequent runs, indicating that the catalyst could be utilized at least five times. It was similar to previous studies (Luo et al., 2015; Shi et al., 2012). Meanwhile, the reaction solution after the first cycle was collected and filtrated to detect the leaching concentrations of Mn ions and Fe ions. As seen in Fig. 6(C–D), the leaching of Mn ions in the solution was 0.54 mg/L, and no iron ion was detected. The leaching of Mn and Fe ions was very few, indicating that the metal precipitation of MnFe-LDH and the loss of catalyst activity could be neglected. Besides, the full survey scan spectra of MnFe-LDH before and after reaction was nearly same and no obvious changes (Fig. 9(C)), which confirmed the excellent stability of MnFe-LDH. The study strongly suggested that the catalyst of MnFe-LDH owned high reusability and excellent stability, which was caused by its layered structure. They were essential for long-term practical implementation in the heterogeneous catalytic system.

4. Conclusions

In summary, a simple, highly efficient and environmental-friendly MnFe-LDH/PMS system was reported and excellent dye removal was achieved. The experimental results testified that MnFe-LDH could act as an efficient PMS activator. >97.00% of AO7 could be degraded within 30 min when the dosage of catalyst and PMS were both 0.20 g/L and the AO7 concentration was 20 mg/L. The calculated rox (molar ratio of PMS/pollutant) of MnFe-LDH/PMS system was 5.87, which was much lower than other Fe/Mn based catalysts/PMS system (Table S2), implying that MnFe-LDH/PMS system had relatively strong oxidizing property for organic pollutants with lesser oxidant usage.

The high-oxidative ability of resulting $SO_4^{\bullet-}$ and •OH was the crucial reason for the improved AO7 degradation rate, which could be confirmed by ESR and quenching tests. Moderate increase of PMS concentration, catalyst dosage and reaction temperature all presented positive effects on AO7 degradation, and neutral solution was more beneficial for the degradation. In addition, the prepared MnFe-LDH also displayed high reusability and excellent stability of lower metal ions dissolution, further to confirm its actual application potentials. Based on the UV–vis spectrum and GC–MS analysis of intermediates, the probable pathways of AO7 degradation were presented, involving the cleavages of azo bonds, the generations of phenyl and naphthalene products and the openings of rings. This work suggests that MnFe-LDH could act as an effective candidate for activating PMS to remove organic contaminants.

Acknowledgments

This work was partially supported by the National Natural Science Foundation of China (No. 51779088, 51779089 and 51478170), Planned Science and Technology Project of Hunan Province (No. 2017WK2091), Postdoctoral Innovation Talent Support Program of China (No. BX20180290) and the China Postdoctoral Science Foundation (Grant No. 2018M640595).

Appendix A. Supplementary data

Supplementary data to this article can be found online at https://doi.org/10.1016/j.scitotenv.2019.01.190.

References

Abdelkader, B.H., Bentouami, A., Derriche, Z., Bettahar, N., Ménorval, L.C.D., 2011. Synthesis and characterization of Mg–Fe layer double hydroxides and its application on adsorption of Orange G from aqueous solution. Chem. Eng. J. 169, 231–238.

Ahmadi, M., Ghanbari, F., 2018. Combination of UVC-LEDs and ultrasound for peroxymonosulfate activation to degrade synthetic dye: influence of promotional and inhibitory agents and application for real wastewater. Environ. Sci. Pollut. Res. 25, 6003–6014.

Ahmadi, M., Ghanbari, F., 2019. Organic dye degradation through peroxymonosulfate catalyzed by reusable graphite felt/ferriferrous oxide: mechanism and identification of intermediates. Mater. Res. Bull. 111, 43–52.
Ahmadi, M., Ghanbari, F., Alvarez, A., Martinez, S.S., 2017. UV-LEDs assisted peroxymonosulfate/Fe^{2+} for oxidative removal of carmoisine: the effect of chloride ion. Korean J. Chem. Eng. 34, 2154–2161.
Azam, A., Hamid, A., 2006. Effects of gap size and UV dosage on decolorization of C.I. acid orange 7 by UV/H_2O_2 process. J. Hazard. Mater. 133, 167–171.
Bennekou, P., 2012. Cobalt metabolism and toxicology–a brief update. Sci. Total Environ. 432, 210–215.
Boczkaj, G., Fernandes, A., 2017. Wastewater treatment by means of advanced oxidation processes at basic pH conditions: a review. Chem. Eng. J. 320, 608–633.
Bukhtiyarova, M.V., 2019. A review on effect of synthesis conditions on the formation of layered double hydroxides. J. Solid State Chem. 269, 494–506.
Cai, C., Hui, Z., Xing, Z., Hou, L., 2015. Ultrasound enhanced heterogeneous activation of peroxymonosulfate by a bimetallic Fe–Co/SBA-15 catalyst for the degradation of Orange II in water. J. Hazard. Mater. 283, 70–79.
Chen, D., Ma, X., Zhou, J., Chen, X., Qian, G., 2014. Sulfate radical-induced degradation of acid orange 7 by a new magnetic composite catalyzed peroxymonosulfate oxidation process. J. Hazard. Mater. 279, 476–484.
Chen, F., Yang, Q., Zhong, Y., An, H., Zhao, J., Xie, T., et al., 2016. Photo-reduction of bromate in drinking water by metallic Ag and reduced graphene oxide (RGO) jointly modified $BiVO_4$ under visible light irradiation. Water Res. 101, 555–563.
Dhaka, S., Kumar, R., Lee, S.-H., Kurade, M.B., Jeon, B.-H., 2018. Degradation of ethyl paraben in aqueous medium using advanced oxidation processes: efficiency evaluation of UV-C supported oxidants. J. Clean. Prod. 180, 505–513.
Dong, H., Wei, M., Li, J., Fang, J., Gao, L., Li, X., et al., 2016. Catalytic performance of supported g-C_3N_4 on MCM-41 in organic dye degradation with peroxymonosulfate. RSC Adv. 6, 70747–70755.
Du, J., Bao, J., Ying, L., Ling, H., Han, Z., Sang, H.K., et al., 2016. Efficient activation of peroxymonosulfate by magnetic Mn-MGO for degradation of bisphenol A. J. Hazard. Mater. 320, 150–159.
Fang, J.Y., Shang, C., 2012. Bromate formation from bromide oxidation by the UV/persulfate process. Environ. Sci. Technol. 46, 8976–8983.
Feng, Y., Wu, D., Zhou, Y., Shih, K., 2017. A metal-free method of generating sulfate radicals through direct interaction of hydroxylamine and peroxymonosulfate: mechanisms, kinetics, and implications. Chem. Eng. J. 330, 906–913.
Fu, H., Ma, S., Zhao, P., Xu, S., Zhan, S., 2019. Activation of peroxymonosulfate by graphitized hierarchical porous biochar and $MnFe_2O_4$ magnetic nanoarchitecture for organic pollutants degradation: structure dependence and mechanism. Chem. Eng. J. 360, 157–170.
Furman, O.S., 2010. Mechanism of base activation of persulfate. Environ. Sci. Technol. 44, 6423–6428.
Gerken, J.B., Mcalpin, J.G., Chen, J.Y.C., Rigsby, M.L., Casey, W.H., Britt, R.D., et al., 2011. Electrochemical water oxidation with cobalt-based electrocatalysts from pH 0–14: the thermodynamic basis for catalyst structure, stability, and activity. J. Am. Chem. Soc. 133, 14431–14442.
Ghanbari, F., Moradi, M., 2017. Application of peroxymonosulfate and its activation methods for degradation of environmental organic pollutants: review. Chem. Eng. J. 310, 41–62.
Gong, C., Chen, F., Yang, Q., Luo, K., Yao, F., Wang, S., et al., 2017. Heterogeneous activation of peroxymonosulfate by Fe-Co layered doubled hydroxide for efficient catalytic degradation of Rhoadmine B. Chem. Eng. J. 321, 222–232.
Guo, W., Su, S., Yi, C., Ma, Z., 2013. Degradation of antibiotics amoxicillin by Co_3O_4-catalyzed peroxymonosulfate system. Environ. Prog. Sustain. Energy 32, 193–197.
Guo, Y., Li, J., Gao, Z., Zhu, X., Liu, Y., Wei, Z., et al., 2016. A simple and effective method for fabricating novel p – n heterojunction photocatalyst g-C_3N_4/$Bi_4Ti_3O_{12}$ and its photocatalytic performances. Appl. Catal. B Environ. 192, 57–71.
Hammami, S., Bellakhal, N., Oturan, N., Oturan, M.A., Dachraoui, M., 2008. Degradation of acid orange 7 by electrochemically generated OH radicals in acidic aqueous medium using a boron-doped diamond or platinum anode: a mechanistic study. Chemosphere 73, 678–684.
Hu, J., Dong, H., Qu, J., Qiang, Z., 2017. Enhanced degradation of iopamidol by peroxymonosulfate catalyzed by two pipe corrosion products (CuO and delta-MnO_2). Water Res. 112, 1–8.
Hu, L., Zhang, G., Liu, M., Wang, Q., Dong, S., Wang, P., 2019. Application of nickel foam-supported Co_3O_4-Bi_2O_3 as a heterogeneous catalyst for BPA removal by peroxymonosulfate activation. Sci. Total Environ. 647, 352–361.
Huang, Y.H., Huang, Y.F., Huang, C.I., Chen, C.Y., 2009. Efficient decolorization of azo dye reactive black B involving aromatic fragment degradation in buffered Co^{2+}/PMS oxidative processes with a ppb level dosage of Co^{2+}-catalyst. J. Hazard. Mater. 170, 1110–1118.
Huang, G.X., Wang, C.Y., Yang, C.W., Guo, P.C., Yu, H.Q., 2017. Degradation of bisphenol A by peroxymonosulfate catalytically activated with $Mn_{1.8}Fe_{1.2}O_4$ nanospheres: synergism between Mn and Fe. Environ. Sci. Technol. 51, 12611–12618.
Ji, Y., Dong, C., Kong, D., Lu, J., Zhou, Q., 2015. Heat-activated persulfate oxidation of atrazine: implications for remediation of groundwater contaminated by herbicides. Chem. Eng. J. 263, 45–54.
Jiang, P.Y., Katsumura, Y., Ishigure, K., Yoshida, Y., 1992. Reduction potential of the nitrate radical in aqueous solution. Inorg. Chem. 31, 5135–5136.
Kim, Y.S., 2012. Mn–Fe layered double hydroxides for adsorption of As(III) and As(V). Separation Sci. Tech. 47, 2192–2198.
Kudlich, Michael, ‡, M. J. H., Hansjoachim Knackmuss, A. Andreas Stolz, 2009. Autoxidation reactions of different aromatic o-aminohydroxynaphthalenes that are formed during the anaerobic reduction of sulfonated azo dyes. Environ. Sci. Technol. 33, 251–259.
Liang, H., Sun, H., Patel, A., Shukla, P., Zhu, Z.H., Wang, S., 2012. Excellent performance of mesoporous Co_3O_4/MnO_2 nanoparticles in heterogeneous activation of peroxymonosulfate for phenol degradation in aqueous solutions. Appl. Catal. B Environ. 127, 330–335.
Liu, J., Zhao, Z., Shao, P., Cui, F., 2015. Activation of peroxymonosulfate with magnetic Fe_3O_4–MnO_2 core–shell nanocomposites for 4-chlorophenol degradation. Chem. Eng. J. 262, 854–861.
Liu, J., Yang, Q., Wang, D., Li, X., Zhong, Y., Li, X., et al., 2016. Enhanced dewaterability of waste activated sludge by Fe(II)-activated peroxymonosulfate oxidation. Bioresour. Technol. 206, 134–140.
Lu, H., Zhu, Z., Zhang, H., Zhu, J., Qiu, Y., 2015. Simultaneous removal of arsenate and antimonate in simulated and practical water samples by adsorption onto Zn/Fe layered double hydroxide. Chem. Eng. J. 276, 365–375.
Luo, S., Lian, D., Sun, B., Wei, M., Li, X., Xu, A., 2015. Manganese oxide octahedral molecular sieve (OMS-2) as an effective catalyst for degradation of organic dyes in aqueous solutions in the presence of peroxymonosulfate. Appl. Catal. B Environ. 164, 92–99.
Magagula, B., Nhlapo, N., Focke, W.W., 2009. Mn_2Al-LDH and Co_2Al-LDH-stearate as photodegradants for LDPE film. Polym. Degrad. Stab. 94, 947–954.
Mohammad Ali Zazouli, F.G., Yousefi, Maryam, Madihi-Bidgoli, Soheila, 2017. Photocatalytic degradation of food dye by Fe_3O_4/TiO_2 nanoparticles in presence of peroxymonosulfate the effect of UV sources. J. Environ. Chem. Eng. 170, 2459–2468.
Oh, W.D., Dong, Z., Lim, T.T., 2016. Generation of sulfate radical through heterogeneous catalysis for organic contaminants removal: current development, challenges and prospects. Appl. Catal. B Environ. 194, 169–201.
Qi, C., Liu, X., Ma, J., Lin, C., Li, X., Zhang, H., 2016. Activation of peroxymonosulfate by base: implications for the degradation of organic pollutants. Chemosphere 151, 280–288.
Rastogi, A., Al-Abed, S.R., Dionysiou, D.D., 2009. Sulfate radical-based ferrous–peroxymonosulfate oxidative system for PCBs degradation in aqueous and sediment systems. Appl. Catal. B Environ. 85, 171–179.
Ruixia Yuan, S.N.R., Wang, Zhaohui, Liu, Jianshe, 2011. Effects of chloride ion on degradation of acid orange 7 by sulfate radical based advanced oxidation process implications for formation of chlorinated aromatic compounds. J. Hazard. Mater. 196, 173–179.
Saputra, E., Muhammad, S., Sun, H., Ang, H.M., Tadé, M.O., Wang, S., 2014. Shape-controlled activation of peroxymonosulfate by single crystal α-Mn_2O_3 for catalytic phenol degradation in aqueous solution. Appl. Catal. B Environ. 154-155, 246–251.
Shi, P., Su, R., Wan, F., Zhu, M., Li, D., Xu, S., 2012. Co_3O_4 nanocrystals on graphene oxide as a synergistic catalyst for degradation of Orange II in water by advanced oxidation technology based on sulfate radicals. Appl. Catal. B Environ. 123-124, 265–272.
Su, D., Tang, Z., Xie, J., Bian, Z., Zhang, J., Yang, D., et al., 2019. Co, Mn-LDH nanoneedle arrays grown on Ni foam for high performance supercapacitors. Appl. Surf. Sci. 469, 487–494.
Wang, Y., Sun, H., Ang, H.M., Tadé, M.O., Wang, S., 2015. 3D-hierarchically structured MnO_2 for catalytic oxidation of phenol solutions by activation of peroxymonosulfate: structure dependence and mechanism. Appl. Catal. B Environ. 164, 159–167.
Wang, Y., Zhao, X., Cao, D., Wang, Y., Zhu, Y., 2017. Peroxymonosulfate enhanced visible light photocatalytic degradation bisphenol A by single-atom dispersed Ag mesoporous g-C_3N_4 hybrid. Appl. Catal. B Environ. 211, 79–88.
Wei, Z., Villamena, F.A., Weavers, L.K., 2017. Kinetics and mechanism of ultrasonic activation of persulfate: an in situ EPR spin trapping study. Environ. Sci. Technol. 51, 3410–3417.
Xie, L., Zhong, Y., Xiang, R., Fu, G., Xu, Y., Cheng, Y., et al., 2017. Sono-assisted preparation of Fe(II)-Al(III) layered double hydroxides and their application for removing uranium (VI). Chem. Eng. J. 328, 574–584.
Xiong, X., Sun, B., Zhang, J., Gao, N., Shen, J., Li, J., et al., 2014. Activating persulfate by Fe0 coupling with weak magnetic field: performance and mechanism. Water Res. 62, 53–62.
Yang, B., Tian, Z., Wang, B., Sun, Z., Zhang, L., Guo, Y., et al., 2015a. Facile synthesis of Fe_3O_4/hierarchical-Mn_3O_4/graphene oxide as a synergistic catalyst for activation of peroxymonosulfate for degradation of organic pollutants. RSC Adv. 5, 20674–20683.
Yang, Q., Zhong, Y., Zhong, H., Li, X., Du, W., Li, X., et al., 2015b. A novel pretreatment process of mature landfill leachate with ultrasonic activated persulfate: optimization using integrated Taguchi method and response surface methodology. Process. Saf. Environ. Prot. 98, 268–275.
Yang, S., Xiao, T., Zhang, J., Chen, Y., Li, L., 2015c. Activated carbon fiber as heterogeneous catalyst of peroxymonosulfate activation for efficient degradation of acid orange 7 in aqueous solution. Sep. Purif. Technol. 143, 19–26.
Yang, Q., Wang, S., Chen, F., Luo, K., Sun, J., Gong, C., et al., 2017. Enhanced visible-light-driven photocatalytic removal of refractory pollutants by Zn/Fe mixed metal oxide derived from layered double hydroxide. Catal. Commun. 99, 15–19.
Yao, Y., Xu, C., Yu, S., Zhang, D., Wang, S., 2013. Facile synthesis of Mn_3O_4–reduced graphene oxide hybrids for catalytic decomposition of aqueous organics. Ind. Eng. Chem. Res. 52, 3637–3645.
Yao, Y., Cai, Y., Lu, F., Wei, F., Wang, X., Wang, S., 2014. Magnetic recoverable $MnFe_2O_4$ and $MnFe_2O_4$-graphene hybrid as heterogeneous catalysts of peroxymonosulfate activation for efficient degradation of aqueous organic pollutants. J. Hazard. Mater. 270, 61–70.
Zhang, X., Wang, Y., Li, G., Qu, J., 2006. Oxidative decomposition of azo dye C.I. acid orange 7 (AO7) under microwave electrodeless lamp irradiation in the presence of H_2O_2. J. Hazard. Mater. 134, 183–189.
Zhang, J., Shao, X., Shi, C., Yang, S., 2013. Decolorization of acid Orange 7 with peroxymonosulfate oxidation catalyzed by granular activated carbon. Chem. Eng. J. 232, 259–265.
Zhao, H.Z., Sun, Y., Xu, L.N., Ni, J.R., 2010. Removal of acid orange 7 in simulated wastewater using a three-dimensional electrode reactor: removal mechanisms and dye degradation pathway. Chemosphere 78, 46–51.
Zhao, X., Niu, C., Zhang, L., Guo, H., Wen, X., Liang, C., et al., 2018. Co-Mn layered double hydroxide as an effective heterogeneous catalyst for degradation of organic dyes by activation of peroxymonosulfate. Chemosphere 204, 11–21.
Zhou, Y., Jiang, J., Gao, Y., Ma, J., Pang, S.Y., Li, J., et al., 2015. Activation of peroxymonosulfate by benzoquinone: a novel nonradical oxidation process. Environ. Sci. Technol. 49, 12941–12950.